processes

MDPI

Article

Interlayer Interference Mechanisms During Multi-Layer Commingled Production in Low-Permeability Gas Reservoirs

Honggang Mi [1], Bing Zhang [1], Yu Su [1], Chao Wei [2], Le Sun [1], Bo Wang [1], Tianyu Fu [1] and Chen Wang [3,*]

[1] China United Coalbed Methane Corporation Ltd., Beijing 100016, China; hmizlmcq@163.com (H.M.); bzhangzlmcq@163.com (B.Z.); ysuzlmcq@163.com (Y.S.); lsunzlmcq@163.com (L.S.); bwangzlmcq@163.com (B.W.); tyfuzlmcq@126.com (T.F.)
[2] COSL-EXPRO Testing Services (Tianjin) Co., Ltd., Tianjin 300450, China; cweizlmcq@163.com
[3] School of Petroleum Engineering, Xi'an Shiyou University, Xi'an 710065, China
* Correspondence: cwangxsyu@163.com

Abstract

To investigate the interlayer interference mechanism during multi-layer commingled production in low-permeability gas reservoirs, this study focuses on the strongly heterogeneous reservoirs in the central Linxing area of the Ordos Basin. Laboratory-scale physical simulation experiments of commingled production were conducted on core samples from the Shiqianfeng (Q5) and Shihezi (He4) formations, along with the No. 8 + 9 coal seam. The gas production behavior, including the evolution of flow rates, the occurrence of staggered production peaks, and the resulting interlayer interference coefficients, was systematically analyzed and compared between single-layer and multi-layer commingled production scenarios. Experimental results reveal a positive correlation between cumulative gas production and layer permeability under single-layer production conditions. Specifically, the high-permeability layer (0.6470 mD) yielded 65.22 mL, whereas the low-permeability layer (0.1061 mD) produced 36.51 mL, representing a 44.02% reduction relative to the former. Under commingled production conditions, the productivity of the low-permeability layer exhibited more severe inhibition, showing declines in instantaneous production of 34.02–48.96% and cumulative production of 15.50–20.61%. These reductions substantially exceed those observed in the high-permeability layer, which ranged from 6.14% to 6.35% and from 5.00% to 8.76%, respectively. Furthermore, a greater permeability contrast results in a more pronounced difference in gas breakthrough timing. For a permeability ratio of 3, the breakthrough time difference reaches 191 s, compared to 131 s for a ratio of 2. The interlayer interference coefficient exhibits a negative correlation with the permeability contrast. When the contrast is 3, the interference coefficient for the low-permeability layer reaches 79.39%, representing an 84.51% increase relative to the coefficient observed at a contrast of 2. This indicates that larger permeability contrasts lead to more severe interference effects on low-permeability layers. These findings provide theoretical support for optimizing the efficient development of multi-layer commingled production in low-permeability unconventional gas reservoirs, highlighting the necessity of incorporating permeability contrast analysis in commingled production design.

Keywords: low permeability gas reservoir; multi-layer combined mining; interlayer interference

Check for updates

Academic Editor: Albert Ratner

Received: 18 December 2025
Revised: 7 January 2026
Accepted: 9 January 2026
Published: 11 January 2026

Copyright: © 2026 by the authors. Licensee MDPI, Basel, Switzerland. This article is an open access article distributed under the terms and conditions of the Creative Commons Attribution (CC BY) license.

1. Introduction

As a low-carbon, environmentally friendly, and high-quality energy source, natural gas plays a crucial role in the transformation of China's energy structure and the advancement of its ecological civilization [1]. Driven by the growing economic and social demand for clean energy, natural gas consumption has been expanding continuously, with its share in the primary energy mix rising substantially. This growth helps alleviate environmental pressures from excessive coal use, thereby providing a critical pathway for air pollution control and the achievement of carbon neutrality goals [2,3]. However, China's natural gas supply–demand balance continues to face significant challenges. Since 2018, China's external dependence on natural gas has exceeded 40%, heightening concerns over energy security risks [4,5]. Consequently, enhancing the exploration and development of domestic unconventional gas resources has become a strategic imperative for ensuring national energy security. Among these resources, low-permeability sandstone gas and coalbed methane are particularly significant. They are characterized by wide distribution and substantial reserves, yet their reservoirs typically exhibit low porosity and low permeability, making them challenging to develop effectively [6]. Multi-layer commingled production technology serves as a key approach to improving the development efficiency of low-permeability gas reservoirs. This method significantly reduces development costs by producing multiple target layers simultaneously through a single well [7]. However, the effectiveness of this technique is significantly constrained by interlayer interference. This phenomenon refers to the mutual production inhibition and dynamic interaction between layers arising from property contrasts during commingled production [8]. Consequently, investigating the formation mechanisms and dynamic behaviors of interlayer interference in multi-layer commingled production is of both urgent theoretical importance and critical practical value for the efficient development of such low-permeability reservoirs [9].

Extensive research has been conducted on interlayer interference during multi-layer commingled production in oil and gas reservoirs. These studies have established various methodologies, including physical simulation [10], numerical simulation [11], and dynamic data analysis [12], leading to a systematic understanding of interference mechanisms in high-permeability conventional reservoirs [13]. However, existing understanding demonstrates limited applicability to China's extensively distributed continental low-permeability sandstone gas reservoirs and coal-measure gas reservoirs. For instance, existing models typically assume permeability ratios below 5:1, whereas the Linxing area reservoirs exhibit ratios exceeding 10:1, with permeability ranging from 0.01 mD to 2.0 mD based on field data [14]. This represents a 100% discrepancy in degree of heterogeneity compared to conventional reservoirs. This is particularly evident for the strongly heterogeneous, complex lithology low-permeability gas reservoirs in the central Linxing area, where current knowledge shows significant limitations [15–17]. The reservoirs in the central Linxing area exhibit significant heterogeneity in key properties, including permeability contrasts, pore structure, fluid saturation, and pressure retention capacity. These variations lead to more pronounced interlayer conflicts and more complex interference patterns during commingled production [18,19]. Consequently, a thorough understanding of the interference mechanisms specific to such heterogeneous reservoirs is essential for optimizing development strategies in this region. Three critical research gaps remain to be addressed: (1) Current studies are predominantly confined to single gas reservoir types or idealized two-layer commingled production models. A significant knowledge gap exists regarding the dynamic behavior of three-or-more-layer commingled production involving multi-type reservoir combinations, such as low-permeability sandstone and coalbed methane. (2) Systematic experimental investigations and mechanistic explanations are lacking for the dynamic evolution of interference intensity under different production strategies. Current

experimental studies report interference coefficients ranging from 60% to 85% but lack real-time monitoring at intervals shorter than 30 s, missing critical transient effects that account for up to 20% of production variance [20,21]. (3) Effective real-time monitoring and in-depth analysis of interference dynamics are still insufficient during the critical production phase characterized by continuously declining reservoir pressure. Addressing these gaps is essential for developing effective strategies to manage interlayer interference and optimize recovery in complex, multi-layer gas reservoirs. Therefore, establishing a physical simulation system that accurately represents the geological characteristics of low-permeability gas reservoirs is critical. Such a system is essential for revealing the main controlling factors of interlayer interference and the productivity contribution patterns under various commingled production scenarios, which represent both a key focus and a major challenge in advancing the efficient development of these reservoirs [22,23].

Based on the typical geological background of the highly heterogeneous low-permeability gas reservoir in the central Linxing area of the Ordos Basin, this study selects this region as a typical case, which is characterized by multiple reservoir assemblages and a complex geological evolution history [16,24]. It specifically targets the interlayer interference during multi-layer commingled production from the Shiqianfeng (Q5) and Shihezi (He4) formations, as well as the No. 8 + 9 coal seam. Laboratory-scale physical simulation experiments were conducted to investigate interference mechanisms. This study systematically analyzes variations in gas production rates, the characteristics of staggered production peaks, and the evolution of interlayer interference coefficients. The findings aim to provide theoretical insights for optimizing the efficient development of low-permeability unconventional gas reservoirs.

2. Experimental Part

2.1. Experimental Principle

To investigate the mechanisms of interlayer interference during multi-layer commingled production in low-permeability gas reservoirs, this study developed an experimental system based on physical simulation. Core samples from the Shiqianfeng (Q5) and Shihezi (He4) formations, as well as the No. 8 + 9 coal seam in the Linxing Central Block, were selected as representative lithologies. These samples were packed to reflect actual permeability contrasts, thereby simulating key reservoir heterogeneity characteristics. An ISCO pump maintained constant initial formation pressure, while depressurization production was conducted at a controlled temperature. The actual reservoir pressure decline during production was simulated by stepwise back-pressure adjustment. Throughout the experiments, a computer-based data acquisition system monitored and recorded real-time dynamic changes in gas flow rate and pressure at the outlet of each layer. By comparing and analyzing the instantaneous and cumulative gas production, as well as the pressure drop characteristics of each layer under both single-layer and commingled production conditions, the production variation patterns and the degree of interlayer interference under different permeability combinations were revealed.

In multi-layer commingled production, the interference coefficient serves as a key parameter for quantifying interlayer interactions. It specifically measures the degree to which the production performance of a given layer is affected by other producing layers within the same well. A higher interference coefficient indicates a greater degree of interference [24–26]. Essentially, it is defined as the ratio of the actual production performance under commingled conditions to the ideal (or single-layer) production performance without interlayer interference. This relationship is expressed by the following Formula (1):

$$\alpha_{ij} = \frac{q_{i,\,commingled}}{q_{i,\,single}} \quad (1)$$

In the formula, $q_{i,\ commingled}$ is the actual production rate of the *i*-th layer during commingled production with other layers, mL; $q_{i,\ single}$ is the production rate of the *i*-th layer under single-layer production, mL.

2.2. Experimental Apparatus

The experiments employed a physical flow simulation system for multi-layer commingled production, manufactured by Nantong Huaxing Petroleum Instrument Co., Ltd. (Nantong, China). The system incorporated an ISCO 260D metering pump (Lincoln, NE, USA) with a pressure range of 0–51.7 MPa and a continuous flow rate range of 0.001–80 mL/min. A D07 series mass flow meter (Beijing Qixing Huachuang Electronic Co., Ltd., Beijing, China) was used, with a maximum pressure rating of 20 MPa. The flow totalizer (Model D08-8CM) was supplied by Beijing Qixing Huachuang Flowmeter Co., Ltd., (Beijing, China) Pressure was recorded using a KSB20A0R paperless recorder (Ningbo Keshun Instrumentation Co., Ltd. Ningbo, China). The measurement accuracies and uncertainties of these instruments were quantified to ensure data reliability: the ISCO pump had a pressure error of ±0.1% full scale (FS), the mass flow meter exhibited an accuracy of ±0.5% reading (RD), and the temperature controller maintained a stability of ±0.5 °C. These errors were considered in data analysis to minimize their impact on production rate calculations. A schematic diagram of the experimental setup is provided in Figure 1.

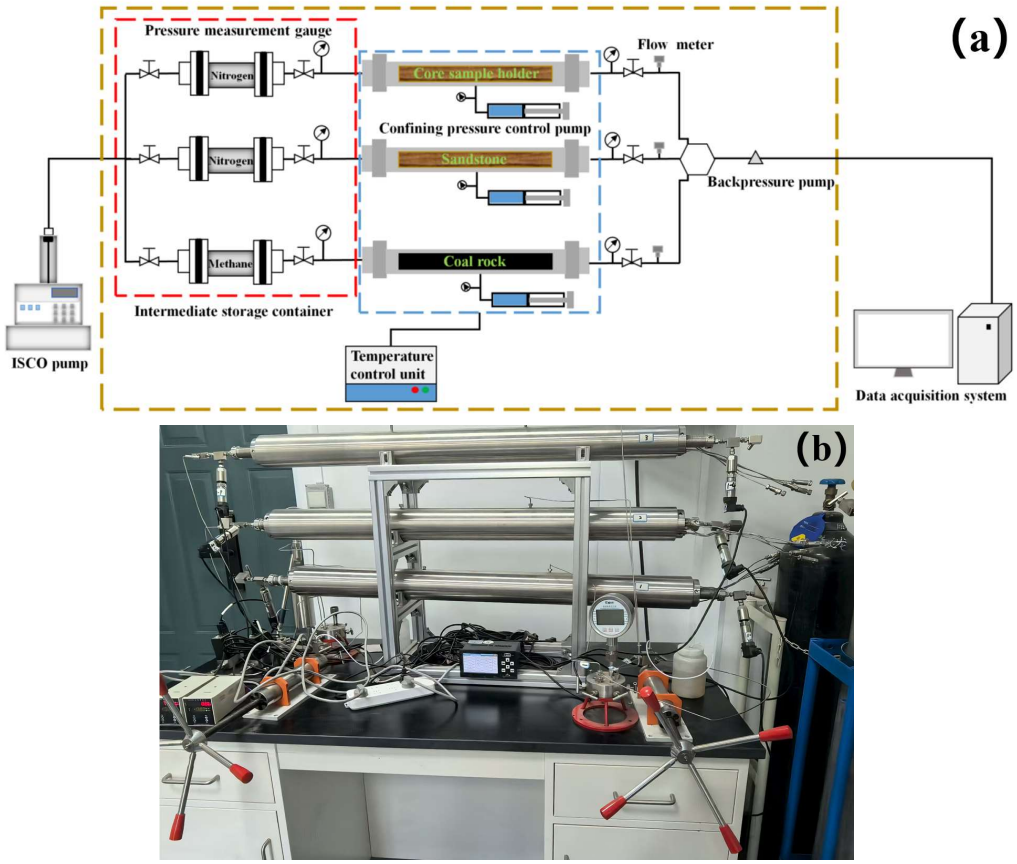


Figure 1. (**a**) Flow chart of gas reservoir commingling experimental device. (**b**) Photograph of the actual experimental setup.

2.3. Experimental Materials

The core samples used in this study are cylindrical, with standardized dimensions of 2.5 cm in diameter and 6.0 cm in length. The sample set comprised 15 sandstone cores from the Shiqianfeng Formation (Q5), 10 sandstone cores from the Shihezi Formation (He4), and

15 coal cores from the No. 8 + 9 coal seam. The measured permeability of the cores ranged from 0.0101 mD to 0.7911 mD, with an average of 0.3302 mD. Porosity varied from 1.20% to 11.29% (average: 6.54%), indicative of strong reservoir heterogeneity. High-purity nitrogen (purity: 99.99%) was used as the experimental gas.

2.4. Experimental Steps

The specific experimental procedure was as follows:

(1) System assembly and leak testing: A multi-layer commingled production simulation system for natural gas was assembled. Prior to experimentation, the sealing integrity of the system was verified by conducting leak tests on all high-pressure pipelines, fittings, and valves.

(2) Core plug preparation and characterization: Twenty core plugs (2.5 cm in diameter × 6.0 cm in length) were drilled from full-diameter cores. The gas permeability of each plug was then measured.

(3) Composite core assembly and permeability testing: The twenty core plugs were sequentially loaded into a long-core holder to simulate the Shiqianfeng (Q5), Shihezi (He4), and coal seam gas layers, resulting in a total composite core length of 100 cm. Following assembly, confining pressure was applied and adjusted to the predetermined value. The permeability of the composite core (representing the reservoir permeability) was then measured.

(4) Core saturation and stabilization: With the outlet valve of the core holder closed, nitrogen was injected into the core through the inlet. The injection pressure, controlled by an ISCO pump via an intermediate container, was increased until a stable pressure of 15 MPa was achieved at both ends of the core holder. The system was then maintained under these saturation conditions for over 8 h to ensure equilibrium.

(5) Production simulation and data acquisition: The experimental temperature was set and maintained at 45 °C. The outlet valves of all simulated gas layers and the commingling manifold valve were then opened to initiate commingled production. Real-time gas flow and pressure data at the outlet were continuously recorded via a computer-based data acquisition and control system.

(6) Depressurization production schedule: The gas reservoir production was simulated under a continuous depressurization schedule. Starting from an initial pressure of 15 MPa, the back pressure was reduced stepwise at 3 MPa intervals based on production time. The minimum back pressure was set to 3 MPa to simulate conditions in the actual production process. The experiment was terminated, and the system was shut down once the outlet pressure declined to the abandonment pressure (approximately 10% of the initial flowing pressure).

(7) Experimental matrix and execution sequence: Following the experimental design, a total of five experiments were conducted: three involving single-layer production simulation and two involving two-layer commingled production simulation. The single-layer experiments were performed first to establish baseline (standard) data. Subsequently, multi-layer commingled production experiments were conducted, and their results were compared against this baseline.

2.5. Experimental Design

Based on the targeted permeability contrasts, a series of experiments was designed, including three groups of single-layer production tests and two groups of two-layer commingled production tests. This design enabled the investigation of commingled production behavior in reservoirs with varying permeability, specifically aiming to elucidate the production dynamics between different low-permeability sandstone gas layers, as well as

between low-permeability sandstone and low-permeability coal-measure gas layers. The specific experimental matrix is detailed in Table 1.

Table 1. Multilayer commingling experimental scheme design.

Experiment Group No.	Type	Combination Principle	Formation	Experimental Pressure/MPa (Reservoir Pressure)	Gas Permeability/mD	Contrast Ratio	Lithology
1	Single-layer	Single-layer Control	Q5	15	0.6470	/	Sandstone
2	Single-layer	Single-layer Control	He4	15	0.2120	/	Sandstone
3	Single-layer	Single-layer Control	8 + 9#	15	0.1061	/	Coal seam
4	Two-layer Commingled	Tight Gas—Coalbed Methane	He4	15	0.2120	2	Sandstone
			8 + 9#	15	0.1061		Coal seam
5	Two-layer Commingled	Tight Gas—Coalbed Methane	He4	15	0.2120	3	Sandstone
			Q5	15	0.6470		Sandstone

3. Experimental Results and Discussion

3.1. Yield Change Rule

According to the experimental matrix detailed in Table 1, single-layer production experiments were conducted on the Q5, He4, and No. 8 + 9 coal seam intervals. Instantaneous and cumulative gas production data for each interval were monitored and recorded using the multi-layer physical flow simulation system. These data were then systematically analyzed to elucidate the dynamic production behavior under varying permeability conditions [27,28].

Figure 2 illustrates the dynamic characteristics of instantaneous and cumulative gas production during the four-stage depressurization process in the Q5 layer. As shown in Figure 2a, each stepwise reduction in back pressure induces a distinct peak in the instantaneous gas production rate. The corresponding peak instantaneous production rates were 129.51 mL, 64.76 mL, 29.79 mL, and 11.91 mL, respectively. Figure 2b demonstrates that the cumulative gas production increases in a stepwise manner corresponding to the alternating opening and closing of the well, while the rate of increase gradually declines. The gas production process concluded at 825 s when the reservoir pressure declined to the abandonment pressure, yielding a final cumulative gas production of 65.22 mL. The kinetics of gas production, evidenced by the sharp peaks following each pressure drop step (Figure 2a), can be attributed to the transient flow regime in low-permeability media. Immediately upon opening the outlet valve, gas from the larger, well-connected pores is rapidly produced, causing a sharp peak. The subsequent rapid decline reflects the quick depletion of this easily accessible gas and the increasing flow resistance from the tighter pore spaces. This peak-and-decline pattern is characteristic of the non-Darcy flow effects under rapid depressurization.

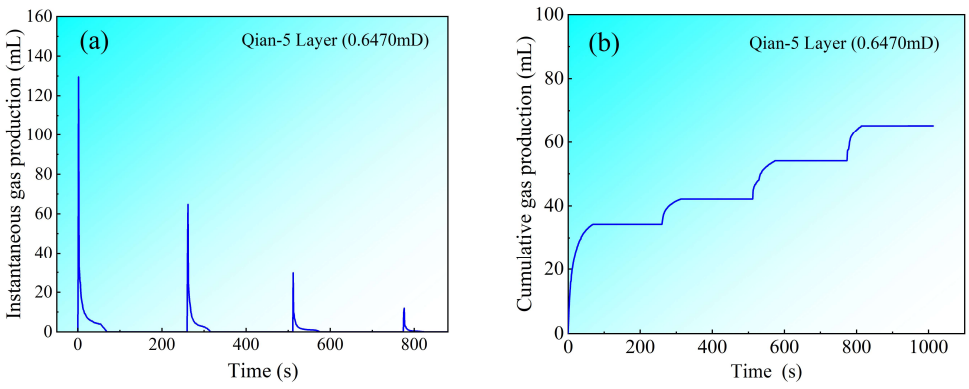


Figure 2. Yield change in Q5 layer. Figure (**a**) shows the instantaneous gas production of Qian-5 layer, and Figure (**b**) shows the cumulative gas production of Qian-5 layer.

Figure 3 illustrates the dynamic characteristics of instantaneous and cumulative gas production during the four-stage depressurization process in the He4 layer. As shown in Figure 3a, the instantaneous gas production rates reached 89.52, 48.20, 11.12, and 2.00 mL/min, respectively. Figure 3b demonstrates that cumulative gas production increases in a stepwise manner in response to the alternating well opening and closing cycles, with a gradually declining rate of increase. The production process concluded at 966 s as the system pressure declined to the abandonment pressure, yielding a final cumulative gas production of 49.52 mL.

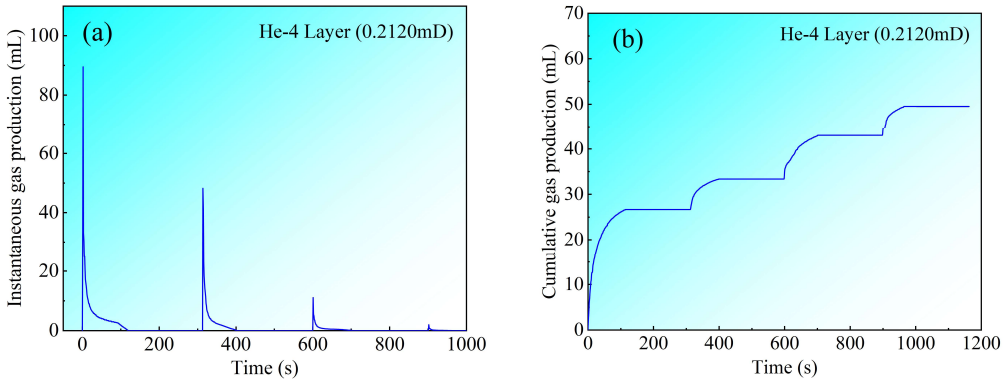


Figure 3. Change in single production yield in He4 layer. Figure (**a**) shows the instantaneous gas production of He-4 layer, and Figure (**b**) shows the cumulative gas production of He-4 layer.

Figure 4 illustrates the dynamic characteristics of instantaneous and cumulative gas production during the four-stage depressurization process in the No. 8 + 9 coal seam. As shown in Figure 4a, the instantaneous gas production rates were 30.56, 12.22, 3.06, and 0.83 mL/min, respectively. Figure 4b demonstrates that the cumulative gas production increases stepwise in response to alternating well opening/closing cycles, while the rate of increase gradually declines. The gas production process concluded at 1140 s when the system pressure declined to the abandonment pressure, yielding a final cumulative production of 36.51 mL.

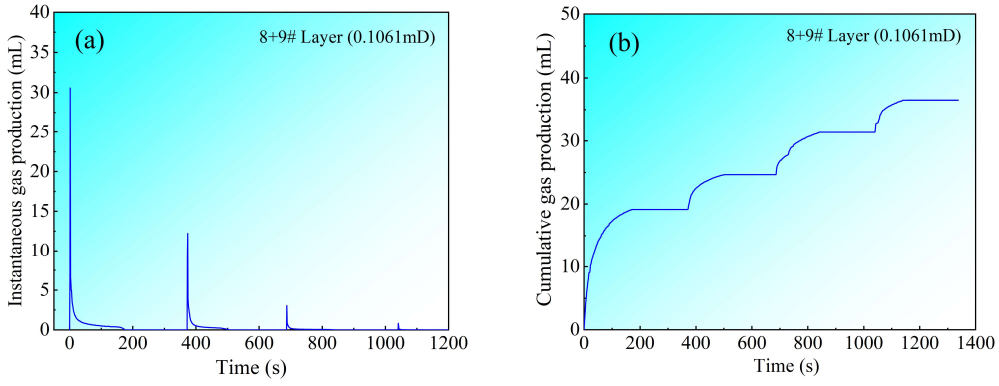


Figure 4. Change in single mining production of 8 + 9# coal seam. Figure (**a**) shows the instantaneous gas production of 8 + 9# layer, and Figure (**b**) shows the cumulative gas production of 8 + 9# layer.

The experimental results indicate that cumulative gas production decreases as reservoir permeability declines. Specifically, production from the high-permeability layer (65.22 mL) was 44.02% greater than that from the low-permeability layer (36.51 mL) (Table 2). This difference is primarily attributed to the narrow pore throats and poor connectivity of seepage pathways in low-permeability reservoirs. Furthermore, repeated opening of the outlet valve accelerates energy dissipation. Coupled with inherently lower

effective reserves and their rapid depletion, these factors lead to a substantial reduction in gas production relative to high-permeability layers. In contrast, high-permeability layers exhibit lower seepage resistance, enabling more efficient and uniform depletion of reserves. Consequently, both instantaneous and cumulative gas production are significantly higher, resulting in a pronounced productivity contrast between the two reservoir types.

Table 2. Quantitative comparison of key production characteristics from single-layer experiments.

Layer	Permeability (mD)	Peak Instantaneous Production (mL/min)	Time to First Peak (s)	Final Cumulative Production (mL)
Q5	0.6470	129.51	60	65.22
He4	0.2120	89.52	120	49.52
8 + 9#	0.1061	30.56	180	36.51

The table compares key production characteristics from single-layer experiments, including peak instantaneous production, time to first peak, and final cumulative production for different layers (Q5, He4, and 8 + 9#). The Q5 layer, with the highest permeability (0.6470 mD), shows the highest peak instantaneous production (129.51 mL/min) and final cumulative production (65.22 mL). It also reaches the first peak the quickest (60 s), demonstrating its greater flow capacity. In contrast, the He4 layer, with lower permeability (0.2120 mD), has lower peak production (89.52 mL/min) and cumulative production (49.52 mL), with a delayed first peak at 120 s. The 8 + 9# coal seam, with the lowest permeability (0.1061 mD), exhibits the slowest gas production, with a peak of only 30.56 mL/min and a final cumulative production of 36.51 mL, taking 180 s to reach the first peak. These results emphasize the significant impact of permeability on gas production, with higher permeability layers yielding more gas both instantaneously and cumulatively.

Following the experimental design outlined in Table 1, two sets of two-layer commingled production experiments were conducted, pairing the He4 layer with the Q5 layer and with the No. 8 + 9 coal seam, respectively. Instantaneous and cumulative gas production data for each layer were monitored and recorded throughout the experiments using the multi-layer physical flow simulation system. A comparative analysis was then performed to quantify the interlayer interference effects under these two distinct permeability and lithology combinations.

Figure 5 illustrates the dynamic changes in instantaneous gas production during two-layer commingled production. The peak instantaneous production for each layer exhibits a significant declining trend over time. Compared to single-layer production, instantaneous gas production during commingled production is substantially lower. This decline occurs because the high-permeability layer, with its lower seepage resistance, preferentially utilizes the system's energy. This diverts and preempts energy that would otherwise be available to the low-permeability layer. Such interlayer channeling significantly reduces the utilization efficiency of the effective reserves in each layer, ultimately leading to the overall decrease in instantaneous productivity observed in all layers [29].

As shown in Figure 5a, when the Q5 and He4 layers are produced commingled, the instantaneous gas production rates for the Q5 layer are 128.41, 60.35, 25.11, and 7.11 mL, representing a 6.35% reduction compared to its average instantaneous production under single-layer conditions. For the He4 layer, the corresponding rates are 62.66, 21.93, 13.16, and 1.77 mL, corresponding to a 34.02% decrease relative to its single-layer production average. Figure 5b presents the results for the He4 and No. 8+9 coal seam commingled pair. The instantaneous production rates for the He4 layer are 88.46, 37.16, 14.12, and 1.87 mL, indicating a 6.14% reduction versus its single-layer baseline. For the No. 8 + 9 coal seam,

the rates are 15.89, 5.88, 1.66, and 0.39 mL, reflecting a more substantial decrease of 48.96% relative to its single-layer production.

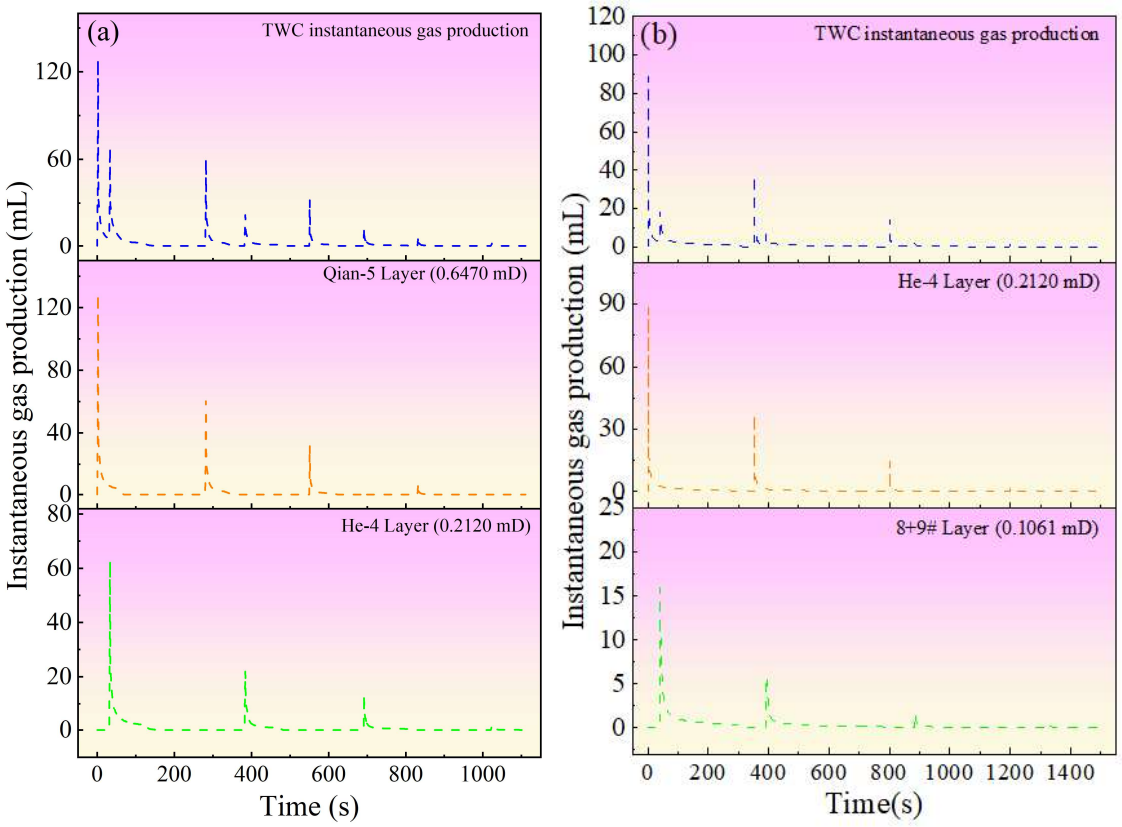


Figure 5. Change in instantaneous gas production in double-layer commingled production. Figure (**a**) shows the instantaneous gas production when Qian-5 and He-4 layers are jointly mined, and Figure (**b**) shows the instantaneous gas production when 8 + 9# and He-4 layers are jointly mined.

Figure 6 illustrates the trend in cumulative gas production for the two-layer commingled production cases. For each layer, cumulative production increased stepwise over time, with the rate of increase gradually declining. As shown in Figure 6a, for the Q5-He4 layer pair, the final cumulative gas production was 59.51 mL and 39.31 mL for the Q5 and He4 layers, respectively. Compared to their theoretical single-layer production, the actual cumulative production of the Q5 layer decreased by 8.76%, while that of the He4 layer decreased by 20.61%. Figure 6b presents the results for the He4 and No. 8 + 9 coal seam pair. The final cumulative production values were 47.04 mL for the He4 layer and 30.85 mL for the coal seam. Relative to their respective theoretical baselines, the He4 layer experienced a 5.00% reduction, and the No. 8 + 9 coal seam experienced a 15.50% reduction in actual cumulative production.

Tight sandstone gas and coalbed methane differ fundamentally in their reservoir architecture and accumulation mechanisms. Tight sandstone gas is primarily hosted in intergranular pores, dissolution pores, and fractures, where gas occurs predominantly as free gas, and it is mainly thermogenic in origin, generated from adjacent source rocks and subsequently accumulated through migration. In contrast, coalbed methane is stored within the coal matrix micropore and cleat system, dominated by an adsorbed phase, and it is characterized by in situ generation and in situ storage. Under commingled production, the relatively higher early-time deliverability of the tight sandstone interval tends to dominate wellbore flow and elevate bottomhole flowing pressure, thereby reducing the effective pressure drawdown and desorption driving force in the coal seam. Together with interlayer

pressure coupling and productivity competition, these effects suppress gas production from the coal seam.

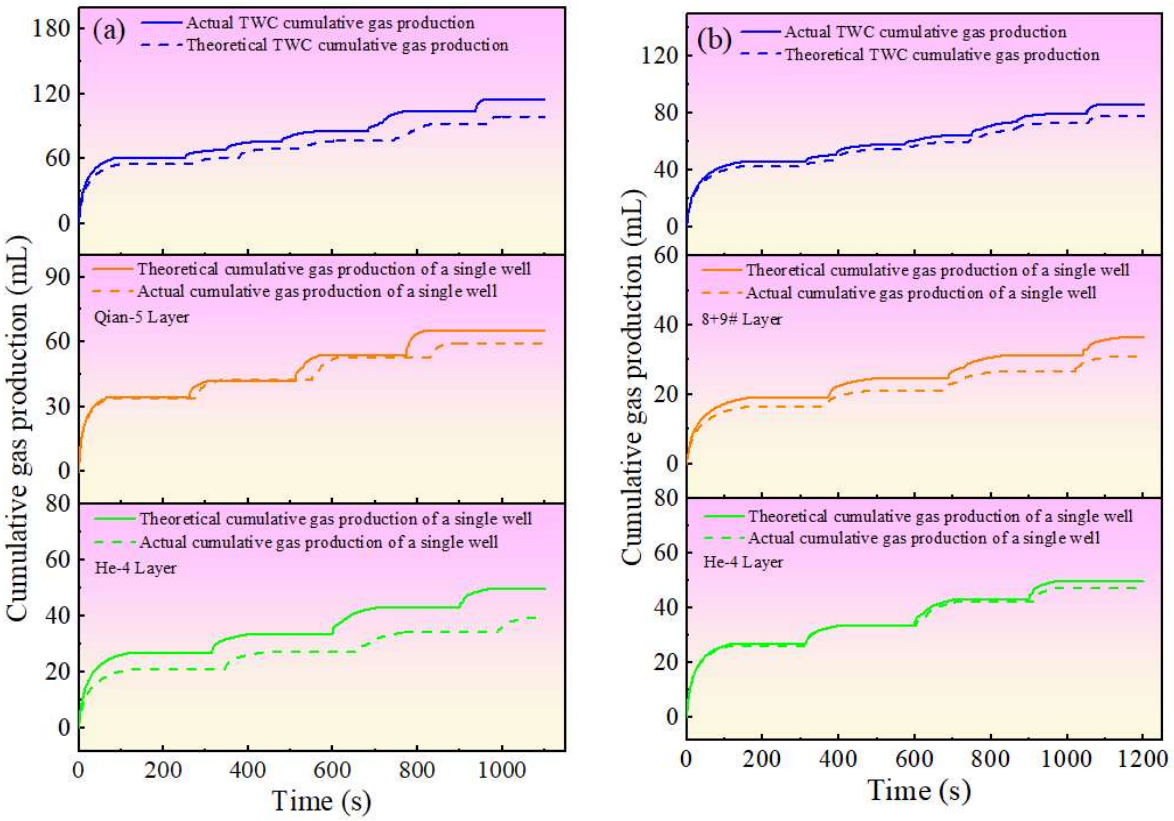


Figure 6. Change in cumulative gas production in double-layer commingled production. Figure (**a**) shows the cumulative gas production when Qian-5 and He-4 layers are jointly produced, and Figure (**b**) shows the cumulative gas production when 8 + 9# and He-4 layers are jointly produced.

The behavior of gas release, as depicted by the cumulative production curves in Figure 6, can be described using a kinetic model based on first-order decay dynamics. The cumulative production (Q(t)) over time (t) follows an exponential approach to a maximum value, $Q(t) = Q_{max}(1 - e^{-kt})$, where Q_{max} is the theoretically recoverable gas volume, and k is the decay constant inversely related to the layer's permeability. This model explains the gradual decline in the rate of increase: lower-permeability layers (e.g., He4) exhibit smaller k values, resulting in slower accumulation, while higher-permeability layers (e.g., Q5) have larger k, leading to faster initial accumulation. The permeability contrast amplifies this difference, as seen in the widening gap between curves in Figure 6b. The results indicate that a larger permeability ratio leads to a more pronounced inhibitory effect from the high-permeability layer on the low-permeability layer.

3.2. The Law of Staggered Peak Gas Production

Figure 7 illustrates the characteristics of instantaneous production peaks and their time-shift behavior under different permeability ratios during two-layer commingled production. This phenomenon arises from differences in interlayer flow capacity, which lead to fluid flow imbalance and distinct pressure transient evolution profiles between the layers. During early production, the high-permeability layer exhibits lower flow resistance, allowing gas to flow rapidly into the wellbore and become the primary contributor to total production. In contrast, narrow flow channels in the low-permeability layer impede gas flow, resulting in a lower contribution to overall production. Consequently, a greater permeability contrast exacerbates interlayer interference. The high conductivity of the

high-permeability layer suppresses production from the low-permeability layer, ultimately leading to the observed staggered production peaks.

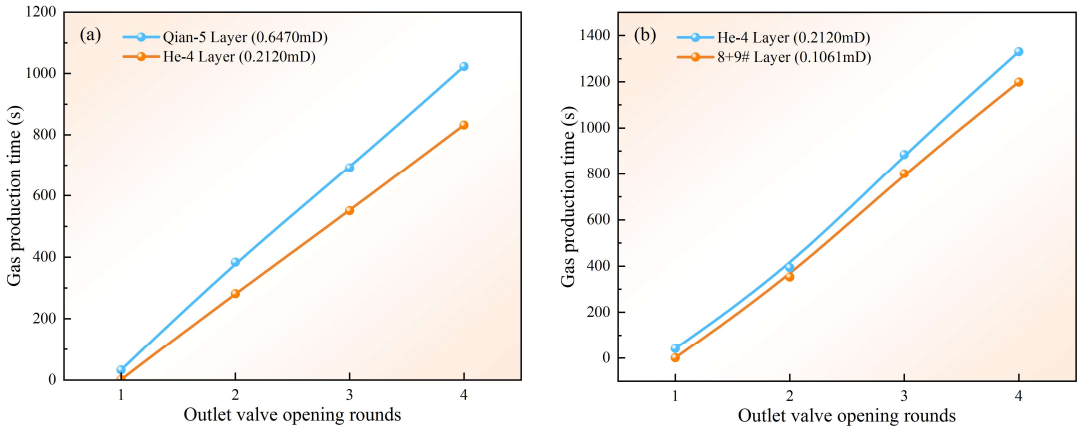


Figure 7. Gas breakthrough timing under different permeability contrasts during two-layer commingled production. Figure (**a**) shows the instantaneous gas production time change of Qian-5 and He-4 layers, and Figure (**b**) shows the instantaneous gas production time change of 8 + 9# and He-4 layers.

In multi-layer commingled production, the timing difference in instantaneous gas production initiation is primarily governed by reservoir heterogeneity, the permeability contrast between layers, and the dynamic competition mechanism during fluid migration. Analysis of the experimental data reveals that the higher-permeability layer initiates gas production earlier, whereas the low-permeability layer exhibits a significant production lag. For the Q5-He4 commingled pair, gas production from the Q5 layer commenced at 2 s, while a noticeable onset for the He4 layer occurred at 33 s. Over time, this initial time gap progressively widened, culminating in a final difference of 191 s between the production peaks of the two layers. For the He4 and No. 8 + 9 coal seam commingled pair, a substantial initial time difference exists in production onset. This time gap progressively widens, resulting in a final difference of 131 s. Analysis indicates that the permeability contrast causes gas to preferentially enter the higher-permeability pathways during flow, forming a dominant flow channel. This preferential flow is a key driver of the staggered production peak phenomenon. Furthermore, as production continues, pressure equilibrium is gradually re-established between the layers. Notably, a greater permeability contrast results in a more pronounced time lag in gas production.

3.3. Variation in Interference Coefficient

Figure 8 presents the variation in the interlayer interference coefficient as a function of permeability contrast for the two-layer commingled production cases. The contrast in reservoir permeability fundamentally creates a disparity in flow capacity between the layers. During commingled production, the wellbore establishes a unified pressure sink. Consequently, the high-permeability layer, characterized by lower flow resistance, experiences faster flow velocities. This leads to a more rapid and extensive expansion of its pressure depletion front, which effectively shields and restricts flow from the low-permeability layer. This shielding effect constricts the effective gas supply area of the low-permeability layer and elevates its flow resistance towards the wellbore, leading to a significant decrease in its interference coefficient. In contrast, the high-permeability layer experiences a relatively minor reverse interference effect from the low-permeability layer, allowing its interference coefficient to remain at a high level. Consequently, a larger permeability contrast results in more severe superposition of interference within the

interlayer flow field, thereby amplifying the disparity in interference coefficients between the layers [30,31].

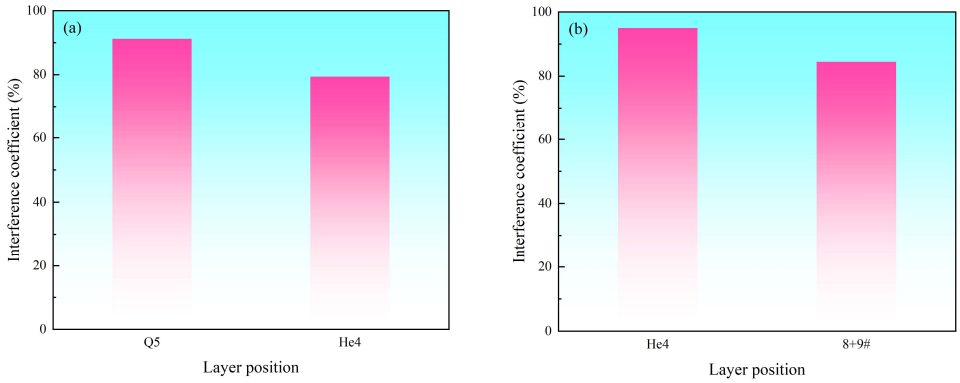


Figure 8. Interference coefficient under different permeability ranges in double-layer commingled production. Figure (**a**) shows the interference coefficient when Qian-5 and He-4 layers are jointly mined, and Figure (**b**) shows the interference coefficient when 8 + 9# and He-4 layers are jointly mined.

The experimental data reveal that for the He4-Q5 layer pair with a permeability contrast of 3, the interference coefficients are 91.24% and 79.39% for the He4 and Q5 layers, respectively. For the He4 and No. 8 + 9 coal seam pair with a contrast of 2, the coefficients are 95.01% for the He4 layer and 84.51% for the coal seam. This indicates that the interference coefficient for the higher-permeability layer consistently exceeds that of its lower-permeability counterpart, and the disparity between the coefficients widens as the permeability contrast increases.

The analysis indicates that an increase in the permeability contrast corresponds to a decrease in the interference coefficient for the low-permeability layer, signifying an enhanced degree of interlayer interference. For the He4 layer, its interference coefficient is 79.39% when commingled with the Q5 layer, compared to 95.01% when commingled with the No. 8 +9 coal seam. Moreover, the high-permeability Q5 layer exhibits a significantly higher interference coefficient (91.24%) than the lower-permeability No. 8 + 9 coal seam (84.51%). This demonstrates that the lower-permeability layer experiences more pronounced interference during commingled production. This is because the high-permeability layer possesses greater flow capacity, enabling a rapid pressure drawdown early in production. This, in turn, further constrains fluid supply from the low-permeability layer, leading to non-uniform pressure distribution and intensified cross-layer interference [32–34].

4. Conclusions

This study focuses on the strongly heterogeneous, low-permeability gas reservoirs in the central Linxing area of the Ordos Basin. To investigate interlayer interference during multi-layer commingled production from the Shiqianfeng (Q5) and Shihezi (He4) formations and the No. 8 + 9 coal seam, laboratory-scale physical simulation experiments were systematically conducted. The main findings are summarized as follows:

(1) Under single-layer production conditions, cumulative gas production is strongly positively correlated with permeability. The high-permeability Q5 layer (0.6470 mD) produced 65.22 mL, which is 44.02% greater than the 36.51 mL produced from the lowest-permeability coal seam (0.1061 mD). This disparity fundamentally results from the lower flow resistance and more efficient pressure depletion in the high-permeability layer, which enables a larger connected pore volume to be effectively drained.

(2) Commingled production exacerbates the productivity disparity between layers, with the low-permeability layer being severely inhibited. A striking contrast is observed:

the high-permeability layer experienced only minor declines in instantaneous (6.14–6.35%) and cumulative production (5.00–8.76%), whereas the low-permeability layer suffered substantial reductions of 34.02–48.96% and 15.50–20.61%, respectively. These results demonstrate that this is primarily due to preferential pressure drawdown and the formation of a dominant flow path in the high-permeability layer, which effectively shields the adjacent low-permeability layer and drastically reduces its effective drainage area.

(3) The permeability contrast governs the temporal production dynamics, resulting in a staggered production peak. A larger contrast significantly increases the time lag for the low-permeability layer to initiate production (e.g., a gap of 191 s for a contrast of 3 compared to 131 s for a contrast of 2). This staggered production phenomenon underscores the competitive flow dynamics and the challenge of achieving simultaneous production from layers with divergent flow capacities.

(4) The interference coefficient serves as an effective metric for quantifying interference intensity, exhibiting a clear negative correlation with permeability contrast. The marked decrease in the coefficient for the low-permeability layer with increasing contrast highlights its greater vulnerability and provides a quantitative tool for predicting interference in similar reservoir configurations.

(5) This study provides a critical practical implication for optimizing commingled production in heterogeneous reservoirs. The experimental quantification reveals a significant overall recovery loss attributable to interlayer interference—approximately 13.9% at a permeability contrast of ~3. This finding indicates the existence of a permeability contrast threshold (between 2 and 3, based on our dataset), beyond which the economic benefit of drilling a single well is substantially compromised by the loss in ultimate recovery. Consequently, for layers with a significant permeability contrast (e.g., >2), commingled production should not be the default strategy. Instead, mitigation techniques such as staged fracturing or sequential production are recommended to control interference and maximize overall recovery efficiency.

5. Limitations

This study elucidates key mechanisms of interlayer interference through controlled physical simulation; however, several limitations inherent to the experimental simplifications should be acknowledged.

(1) Simplification of Flow Dimension: The experiment employed a 1D linear flow model, which differs significantly from the 3D radial flow regime near a wellbore in an actual reservoir in terms of pressure propagation and drainage area. Wellbore storage and skin effects, which play important roles in field production dynamics, were not included in this model.

(2) Simplification of Dynamic Rock Properties: The experiments were conducted under constant confining pressure, assuming invariant core permeability. However, during actual reservoir depletion, increasing effective stress due to a decline in pore pressure can induce stress-sensitive permeability reduction in low-permeability rocks. This effect was not considered, potentially leading to an overestimation of late-stage productivity during commingled production.

(3) Simplification of the Fluid System: The experimental fluid system utilized pure nitrogen, which fundamentally differs from actual reservoir gas in composition and phase behavior. This simplification neglects critical factors, including the presence of formation water, gas–water two-phase flow effects, and the impact of real gas relative permeability under reservoir conditions.

6. Future Work

Building on the findings of this study, future research will focus on three key directions to enhance the practical application of the results:

(1) Numerical Simulation for Field Prediction: We will develop calibrated numerical models using commercial software (e.g., CMG, Eclipse) to upscale the laboratory mechanisms to field conditions. This will enable forecasting long-term production and optimizing development strategies under realistic geological and economic constraints.

(2) Advanced Experiments on Control Strategies: The experimental work will be expanded to investigate three-layer commingled systems and evaluate mitigation strategies, such as sequential and rate-controlled production, under more realistic conditions, including the presence of formation water.

(3) Model Validation with Field Data: A critical step will be to collect and analyze production data from actual commingled wells in the Linxing area. This data will be used to validate and refine the numerical models, ensuring their reliability for field application.

Author Contributions: Conceptualization, H.M.; methodology, B.Z.; formal analysis, Y.S.; investigation, L.S.; resources, B.W.; data curation, T.F.; writing—original draft preparation, C.W. (Chao Wei); writing—review and editing, C.W. (Chen Wang). All authors have read and agreed to the published version of the manuscript.

Funding: This research was supported by the 14th Five-Year Plan Major Project (Key Technologies for Onshore Unconventional Natural Gas Exploration and Development) (KKGG-2021-1000), the National Natural Science Foundation of China (No. 52374041), the Key Research and Development Projects of Shaanxi Province (No. 2023-YBGY-306), and the Key Research Project of Shaanxi Provincial Department of Education (No. 22JY054).

Data Availability Statement: The data that support the findings of this study are available from the corresponding author upon reasonable request.

Conflicts of Interest: Authors Yu Su, Bing Zhang, Honggang Mi, Bo Wang, Le Sun and Tianyu Fu were employed by the China United Coalbed Methane Corporation Ltd. Author Chao Wei was employed by the COSL-EXPRO Testing Services (Tianjin) Co., Ltd. The remaining authors declare that the research was conducted in the absence of any commercial or financial relationships that could be construed as a potential conflict of interest.

References

1. Gajanan, K.; Ranjith, P.G.; Yang, S.Q.; Xu, T. Advances in Research and Developments on Natural Gas Hydrate Extraction with Gas Exchange. *Renew. Sustain. Energy Rev.* **2024**, *190*, 114045. [CrossRef]
2. Skelly, B.P.; Rota, C.T.; Kolar, J.L.; Stillings, B.A.; Edwards, J.W.; Foster, M.A.; Williamson, R.M.; Millspaugh, J.J. Mule Deer Mortality in the Northern Great Plains in a Landscape Altered by Oil and Natural Gas Extraction. *J. Wildl. Manag.* **2024**, *88*, e22619. [CrossRef]
3. Camargo, J.T.; White, J.A.; Hamon, F.P.; Fakeye, V.; Buscheck, T.A.; Huerta, N. Managing Reservoir Dynamics When Converting Natural Gas Fields to Underground Hydrogen Storage. *Int. J. Hydrogen Energy* **2024**, *49*, 1261–1273. [CrossRef]
4. Xu, C.; Yang, T.; Wang, K.; Fu, Q.; Ma, S. Gas Extraction of Coal Seam Roof Fractured Zone in China: A Review. *Fuel* **2024**, *357*, 129930. [CrossRef]
5. Wang, Y.; Zhang, Y.; Yang, X.; Dong, J.; Ma, Y. Optimizing Unconventional Gas Extraction: The Role of Fracture Roughness. *Phys. Fluids* **2024**, *36*, 036611. [CrossRef]
6. Mohamed, T.; Mehana, M. Coalbed Methane Characterization and Modeling: Review and Outlook. *Energy Sources Part Recover. Util. Environ. Eff.* **2025**, *47*, 2874–2896. [CrossRef]
7. Zhang, T.; Wang, B.-R.; Zhao, Y.-L.; Zhang, L.-H.; Qiao, X.-Y.; Zhang, L.; Guo, J.-J.; Thanh, H.V. Inter-layer interference for multi-layered tight gas reservoir in the absence and presence of movable water. *Pet. Sci.* **2024**, *21*, 1751–1764. [CrossRef]
8. Zhao, Q.; Li, X.-S.; Chen, Z.-Y.; Xia, Z.-M.; Xiao, C.-W. Numerical Investigation of Production Characteristics and Interlayer Interference during Co-Production of Natural Gas Hydrate and Shallow Gas Reservoir. *Appl. Energy* **2024**, *354*, 122219. [CrossRef]

9. Li, S.; Guo, Y.; Wu, D.; Liu, L.; Zhang, N. Enhanced Gas Production from Silty Clay Hydrate Reservoirs Using Multi-Branch Wells Combined with Multi-Stage Fracturing: Influence of Fracture Parameters. *Fuel* **2024**, *357*, 129705. [CrossRef]
10. Shamlooh, M.; Mansoor, M.; Konwar, L. Novel Production Enhancement Approach—Multi-Stage Acid Frac to Improve Gas Production and Maximize Reserve of the Tight Dolomite Layers in the Bahrain Field. In Proceedings of the SPE International Hydraulic Fracturing Technology Conference and Exhibition, Muscat, Oman, 23–25 September 2025; SPE: Muscat, Oman, 2025; p. D011S002R003.
11. Seier, M.; Archodoulaki, V.-M.; Koch, T. The Morphology and Properties of Recycled Plastics Made from Multi-Layered Packages and the Consequences for the Circular Economy. *Resour. Conserv. Recycl.* **2024**, *202*, 107388. [CrossRef]
12. Geravand, R. Evaluation of Matrix Acidizing Job in a Layered Gas Condensate Carbonate Reservoir Using Deconvolution Analysis of Well Test Data Combined with Production Logging Data Interpretation. *Iran. J. Gas Eng.* **2024**, e251951, in press.
13. Pal, S.K.; Prabhudesai, V.S.; Vinu, R. Catalytic Upcycling of Post-Consumer Multilayered Plastic Packaging Wastes for the Selective Production of Monoaromatic Hydrocarbons. *J. Environ. Manag.* **2024**, *351*, 119630. [CrossRef] [PubMed]
14. Li, Q.; Ren, D.; Wang, H.; Sun, H.; Li, T.; Zhang, H.; Yan, Z.; Zhang, R.; Qu, L. Microscopic Characteristics of Tight Sandstone Reservoirs and Their Effects on the Imbibition Efficiency of Fracturing Fluids: A Case Study of the Linxing Area, Ordos Basin. *Energy Geosci.* **2024**, *5*, 100302. [CrossRef]
15. Qin, Z.; He, Y.; Wang, N.; Zhao, N.; Yao, Z.; Wu, L.; Ding, Y.; Tang, S.; Liu, X. Improved Relative Permeability Models Incorporating Water Film Effects in Low and Ultra-Low Permeability Reservoirs. *Energy Fuels* **2024**, *38*, 16218–16239. [CrossRef]
16. Tao, X.; Okere, C.J.; Su, G.; Zheng, L. Experimental and Theoretical Evaluation of Interlayer Interference in Multi-Layer Commingled Gas Production of Tight Gas Reservoirs. *J. Pet. Sci. Eng.* **2022**, *208*, 109731. [CrossRef]
17. Liu, X.; Qi, H.; Liu, J.; Geng, X.; Zhang, K.; Li, Y. Feasibility Analysis of Commingle Production of Multi-Layer Reservoirs in the High Water Cut Stage of Oilfield Development. *J. Pet. Explor. Prod. Technol.* **2024**, *14*, 2219–2228. [CrossRef]
18. Okere, C.J.; Sheng, J.J.; Fan, L.-K.; Huang, X.-W.; Zheng, L.-H.; Wei, P.-F. Experimental Study on the Degree and Damage-Control Mechanisms of Fuzzy-Ball-Induced Damage in Single and Multi-Layer Commingled Tight Reservoirs. *Pet. Sci.* **2023**, *20*, 3598–3609. [CrossRef]
19. Van Der Haar (Nee Kosten), K.; Haghighi, M. A New Approach for Production Forecasting from Individual Layers in Multi-Layer Commingled Tight Gas Reservoirs. *APPEA J.* **2022**, *62*, S192–S195. [CrossRef]
20. Lu, Y.; He, W.; Wang, J.; Liu, J.; Shi, H.; Yang, D. Experimental Study on Interlayer Interference Characteristics during Commingled Production in a Multilayer Tight Sandstone Gas Reservoir. *Appl. Sci.* **2024**, *14*, 10534. [CrossRef]
21. Liu, G.; Meng, Z.; Luo, D.; Wang, J.; Gu, D.; Yang, D. Experimental Evaluation of Interlayer Interference during Commingled Production in a Tight Sandstone Gas Reservoir with Multi-Pressure Systems. *Fuel* **2020**, *262*, 116557. [CrossRef]
22. Zhang, W.; Li, Y.; Sun, X.; Li, Y.; Li, M.; Gao, S.; Li, Q. Co-Production Strategy and Its Influencing Factors for Stacked Gas Reservoirs. *Fuel* **2026**, *404*, 136171. [CrossRef]
23. Qin, B.; Wang, H.; Li, F.; Liu, D.; Liao, Y.; Li, H. Towards Zero Carbon Hydrogen: Co-Production of Photovoltaic Electrolysis and Natural Gas Reforming with CCS. *Int. J. Hydrogen Energy* **2024**, *78*, 604–609. [CrossRef]
24. Xiao, H.; Liu, R.; Zhang, F.; Lin, C.; Zhang, M. Sedimentary Model Reconstruction and Exploration Significance of Permian He 8 Member in Ordos Basin, NW China. *Pet. Explor. Dev.* **2019**, *46*, 280–292. [CrossRef]
25. Deryaev, A.R.; Scientific Research Institute of Natural Gas of the State Concern "Turkmengas". Geological, industry and technological bases for the design of the development of multi-layer fields by the method of dual completion operation of wells. *Theor. Appl. Sci.* **2023**, *117*, 601–608. [CrossRef]
26. Cui, C.; Liu, Y.; Zhang, G.; Ren, Y.; Chai, X. Research of Productivity and Interlayer Interference Mechanism of Multi-layer Co-Production in Reservoirs with Multipressure Systems. *J. Energy Res. Technol. Part B* **2025**, *1*, 021002. Available online: https://asmedigitalcollection.asme.org/energyresourcessubsurface/article-abstract/1/2/021002/1206992/Research-of-Productivity-and-Interlayer?redirectedFrom=fulltext (accessed on 17 December 2025).
27. Pusarapu, V.; Narayana Sarma, R.; Ochonma, P.; Gadikota, G. Sustainable Co-Production of Porous Graphitic Carbon and Synthesis Gas from Biomass Resources. *npj Mater. Sustain.* **2024**, *2*, 16. [CrossRef]
28. Wang, L.; He, Y.; Wang, Q.; Liu, M.; Jin, X. Improving Tight Gas Recovery from Multi-Pressure System during Commingled Production: An Experimental Investigation. *Nat. Resour. Res.* **2021**, *30*, 3673–3694. [CrossRef]
29. Effect of Interlayer Flow Capability on the Interference of Natural Gas Hydrate and Shallow Gas Reservoir Co-Production—101—Web of Science Core Collection. Available online: https://libresource.xsyu.edu.cn/https/443/cn/clarivate/webofscience/yitlink/wos/woscc/summary/8ce002d7-404f-4917-af5b-33eb339d4924-0191914d7f/b5e856b3-918b-46cb-9244-0262990488ba-0191914d54/relevance/1 (accessed on 17 December 2025).
30. A Numerical Investigation of Gas Flow Behavior in Two-Layered Coal Seams Considering Interlayer Interference and Heterogeneity—101—Web of Science Core Collection. Available online: https://libresource.xsyu.edu.cn/https/443/cn/clarivate/webofscience/yitlink/wos/woscc/summary/2337dcfe-d1fa-4247-ba1b-da4f1b761bf9-01919170ca/99bee911-9d39-43e1-8764-8c00219dc299-01919170ab/relevance/1 (accessed on 17 December 2025).

31. Liu, H.; Gao, S.; Fang, F.; Jiao, C.; Li, Q.; Ye, L.; An, W.; Zhang, J. Model of Cross-Flow Interference Index and Application for Multi-Layer Commingled Production in Sulige Tight Sandstone Gas Reservoir, Ordos Basin, China. *J. Nat. Gas Geosci.* **2023**, *8*, 389–401. [CrossRef]
32. Experimental Study on Improving the Recovery Rate of Low-Pressure Tight Oil Reservoirs Using Molecular Deposition Film Technology—100—Web of Science Core Collection. Available online: https://libresource.xsyu.edu.cn/https/443/cn/clarivate/webofscience/yitlink/wos/woscc/summary/285204b2-1ff4-475c-acab-726204574519-01919223d7/a7ff6435-c51f-4e11-81f0-47486f79dbcf-0191922388/relevance/1 (accessed on 17 December 2025).
33. Hu, W.; Wei, Y.; Bao, J. Development of the Theory and Technology for Low Permeability Reservoirs in China. *Pet. Explor. Dev.* **2018**, *45*, 685–697. [CrossRef]
34. Zhang, J.; Bai, X.; Song, Z.; Zhang, Y.; Dong, X.; Wu, S.; Xing, C.; Li, X.; Xu, W.; Zhang, S. Research Progress and Perspectives on Prevention and Control Technologies for Coal–Rock–Gas Composite Dynamic Disasters: New Types of Induced Classifications, Discriminant Criteria, and Structural Control Schemes. *Rock Mech. Rock Eng.* **2025**, *58*, 10143–10181. [CrossRef]

Disclaimer/Publisher's Note: The statements, opinions and data contained in all publications are solely those of the individual author(s) and contributor(s) and not of MDPI and/or the editor(s). MDPI and/or the editor(s) disclaim responsibility for any injury to people or property resulting from any ideas, methods, instructions or products referred to in the content.